A Bifunctional Platinum(II) Complex Capable of Intercalation and Hydrogen-Bonding Interactions with DNA: Binding Studies and Cytotoxicity

Dik-Lung Ma and Chi-Ming Che*[a]

Abstract: The interactions of [Pt(CNN)(4-dpt)]PF_6, (**1**; 4-dpt = 2,4-diamino-6-(4-pyridyl)-1,3,5-triazine, HCNN = 6-phenyl-2,2′-bipyridine) with double-stranded DNA, poly(dA-dT)$_2$, and poly(dG-dC)$_2$ were examined by spectroscopic, electrophoretic, and hydrodynamic methods. The spectroscopic data were analyzed with McGhee, van′t Hoff, and Gibbs–Helmholtz equations. In a comparative study, [Pt(CNN)(py)]PF_6 (**2**; py = pyridine) was prepared and the nature of its binding towards DNA was investigated [preliminary results: *ChemBioChem* **2003**, *4*, 62–68]. For reactions with calf thymus DNA at 20 °C, the intrinsic binding constants for **1** and **2** are $(4.6 \pm 0.2) \times 10^5$ and $(2.3 \pm 0.3) \times 10^4$ mol^{-1} dm^3, respectively. Results of DNA-binding reactions revealed that **1** and **2** preferentially bind to the AT sequence of duplex DNA. Intercalation is the preferred binding mode for **2**, whereas both intercalation and minor-groove binding are observed for **1**. Complex **1** is cytotoxic against a number of carcinoma cell lines, including KB-3-1, CNE-3, and HepG2, and remains potent against multidrug- or cisplatin-resistant KB-V-1 and CNE1 cell lines, for which the resistance ratios are 1.6 and 1.5, respectively. Importantly, **1** is almost an order of magnitude less toxic to the normal cell line CCD-19Lu ($IC_{50} = 176 \pm 1.7$ μM) and it selectively induced apoptosis leading to cancer cell death with less than 5% detectable necrosis.

Keywords: antitumor agents · bioinorganic chemistry · luminescence · N ligands · platinum

Introduction

In the context of developing metal-based therapeutics and luminescent probes for biomolecules, systematic studies on interactions of biomolecular targets such as DNA and proteins with structurally defined metal complexes at the molecular level can provide useful information.[1–10] Metal complexes are well documented to bind to DNA covalently and noncovalently. Cisplatin is the best known example of the former and binds to DNA by coordination of the Pt atom to the N7 positions of two guanine bases or to adenine and guanine.[3] Noncovalent interactions between metal complexes and DNA include hydrogen bonding, electrostatic interaction, and intercalation. Lippard et al. pioneered studies on DNA–metallointercalators using square-planar d^8 Pt^{II} complexes,[3,4] while Barton et al. subsequently extended the scope to octahedral d^6 metal complexes with aromatic diimine ligands.[1] Thus, $[Ru(diimine)_3]^{2+}$,[1] $[Cu(diimine)_2]^+$,[6,12] and $[Pt(terpy)L]^+$[4,11] (terpy = 2,2′:6′,2″-terpyridine; L = anionic ligand, $n = 1$; L = neutral ligand, $n = 2$) are examples of metal complexes which behave like organic intercalators such as Netropsin,[13,14] Distamycin,[15] and DAPI (4′,6-diamidino-2-phenylindole).[16] These metallointercalators bind to DNA through π–π and electrostatic interactions, and are unlike Hoechst derivatives,[17–19] which are groove binders with crescent shapes and which contain hydrogen-bonding functionalities that permit binding to the convex curvature of minor grooves.

One of our approaches to inorganic pharmaceutical research is to develop metal complexes that bind DNA in a predetermined manner, since such binding may result in modification of critical DNA functions such as replication and transcription. In this regard, we were attracted to the reports by Mingos et al. advocating design studies on metal complexes with nitrogen-donor ligands that can participate in both hydrogen-bonding and π–π interactions for molecular-recognition and crystal-engineering applications.[20] We envisioned that cooperative effects arising from such nonco-

[a] Prof. Dr. C.-M. Che, D.-L. Ma
Department of Chemistry and Open Laboratory of Chemical Biology of the Institute of Molecular Technology for Drug Discovery and Synthesis
The University of Hong Kong
Pokfulam Road, Hong Kong SAR (China)
Fax: (+852) 2857-1586
E-mail: cmche@hku.hk

Supporting information for this article is available on the WWW under http://www.chemeurj.org/ or from the author. Crystallographic data for **2** and 4-dpt; UV/Vis and emission spectra of **2** with increasing concentration of ct DNA; ^{1}H NMR spectra of d(CAATCCGGATTG)$_2$ with increasing concentration of **2**; table of thermodynamic parameters for **1** and **2** with poly(dA-dT)$_2$.

 DOI: 10.1002/chem.200304964

valent interactions would be a valuable principle in the development of new metal-based probes which recognize biomolecular targets with high specificity. $[Pt(CNN)(L)]^+$ (L = neutral ligand) complexes have been reported to display photoluminescence that is sensitive to the local microenvironment,[21,22] and they are structurally related to the well-known intercalator $[Pt(terpy)Cl]^+$.[23] Here we describe studies on DNA binding and cytotoxicity of the cyclometalated platinum(II) complex $[Pt(CNN)(4\text{-dpt})]PF_6$ (**1**) containing a pyridyl ligand that carries a triple hydrogen-bonding motif.

Results

The employment of functionalized organic chromophores/building blocks with complementary hydrogen bonding motifs that are analogous to nucleic acid base pairs is a widely adopted strategy for the construction of supramolecular assemblies and for binding studies on biomolecules.[24] Mingos et al. previously reported the ligand 4-dpt, which contains hydrogen-bonding donor–acceptor–donor (DAD) sites complementary to those of pyrimidine bases.[25] Transition-metal complexes of 4-dpt form hydrogen-bonded molecular assemblies.[20] We conceived that a platinum(II) complex containing a peripheral 4-dpt moiety would form intermolecular complementary hydrogen bonds with biomolecules such as DNA and proteins, while the square-planar $[Pt^{II}(CNN)]$ fragment would be capable of intercalation by π–π interactions. According to the literature, 4-dpt can be prepared by condensation of biguanide with isonicotinamide in alkaline methanol.[25] Complexes **1** and **2** were prepared by treating [PtCl(CNN)] with the corresponding pyridyl ligand in refluxing MeCN/MeOH and were obtained as PF_6^- salts.

A useful probe for the η^3 coordination mode of the CNN ligand are the intensities of the C=C and C=N stretches; both diminish upon complexation to a metal ion. The IR absorption band(s) at about 1600 cm^{-1} of **1** and **2** are thus significantly weaker than that of the free ligand HCNN. The ^1H NMR spectra of **1** and **2** are consistent with the η^3 coordination mode of the ligand, and their positive-ion FAB mass spectra show molecular ion clusters at *m*/*z* 614 and 505, respectively, corresponding to the formulations $[Pt(CNN)(4\text{-dpt})]^+$ and $[Pt(CNN)(py)]^+$.

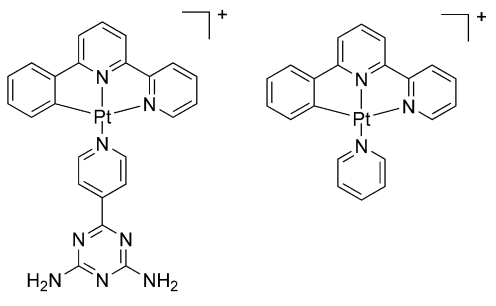

1 **2**

The crystal structure of **2** shows that the Pt atom adopts a distorted square-planar geometry in which the N(1)-Pt(1)-C(1) angle of 161.8(4)° significantly deviates from 180°. The bond angles and distances are comparable to related values in $[Pt(CNN)(MeCN)]^+$.[26] The Pt–N(py) bond length in **2** (2.02(1) Å) is shorter than that in *trans*-$[PtCl_2(py)_2]$ (2.085 Å).[27] The intermolecular Pt···Pt separation in the crystal lattice of **2** is greater than 3.6 Å and thus indicates no significant Pt···Pt interaction between adjacent [Pt(CNN)] moieties, although weak π–π interactions are possible. This is presumably due to the steric effect imposed by the coordinated py ligand, the plane of which is orthogonal to the [Pt(CNN)] moiety.

Spectroscopic properties: The absorption spectrum of **1** in Tris buffer displays three absorption peaks [λ/nm (ε_{max}/$dm^3\,mol^{-1}\,cm^{-1}$): 420 (1100), 320 (1.36×10^4), 268 (4.22×10^4)]. Complex **2** shows a similar UV/Vis absorption spectrum but with an additional peak [λ/nm (ε_{max}/$dm^3\,mol^{-1}\,cm^{-1}$): 420 (1500), 346 (1.07×10^4), 311 (1.11×10^4), 256 (2.40×10^4)]. The broad absorption at 420 nm is assigned to the [(5d)Pt→π*(CNN)] charge-transfer transition (this spectral assignment was previously made for $[Pt(CNN)L]^{n+}$ (L = py, PPh_3, Cl)[28]).

Excitation of **1** (50 μM) at 320 nm in degassed Tris buffer gave an emission with λ_{max} at 547 nm, a quantum yield of 0.035, and a lifetime of 4.0 μs. For **2** (50 μM), a similar emission at 537 nm with a shorter lifetime of 0.3 μs and a quantum yield of 0.004 was found. With reference to previous studies,[28,29] these emissions are ^{3}MLCT [Pt→π*(CNN)] in nature. Minor solvatochromism of the emissions was observed. For example, the emission of **1** (**2**) shifted from 547 (535) nm in acetonitrile to 550 (540) nm in dichloromethane. Self-quenching of the emission was observed for **1** at 298 K in dichloromethane. A linear plot of $1/\tau$ against [complex] was obtained, and a self-quenching rate constant of $k_q = 2.8\times10^8\ mol^{-1}\,dm^3\,s^{-1}$ was derived.

Absorption titration: It is well documented that the transition dipole moment of metal complexes can be affected by binding to DNA grooves or intercalative π–π stacking interactions. As depicted in Figure 1, the absorption spectra of **1** in the presence of calf thymus DNA at various concentrations reveal hypochromism (27%) at 320 nm without significant bathochromic spectral shift. The spectral changes showed clear isosbestic points at 305 and 358 nm throughout the titration experiment.

The intrinsic binding constant K was determined from a plot of $D/\Delta\varepsilon_{ap}$ versus D according to Equation (1),[30]

$$D/\Delta\varepsilon_{ap} = D/\Delta\varepsilon + 1/(\Delta\varepsilon K) \quad (1)$$

where D is the concentration of DNA, $\Delta\varepsilon_{ap} = |\varepsilon_A - \varepsilon_F|$, $\varepsilon_A = A_{obs}/[complex]$, and $\Delta\varepsilon = |\varepsilon_B - \varepsilon_F|$; ε_B and ε_F are the extinction coefficients of the DNA–**1** adduct and unbound complex **1**, respectively. For the absorbance data at 320 nm, the plot of $D/\Delta\varepsilon_{ap}$ versus D (Figure 1, inset) is linear and the K value is $(4.6\pm0.2)\times10^5\ mol^{-1}\,dm^3$. The ε_B value derived from the plot is $3.69\times10^3\ mol^{-1}\,dm^3\,cm^{-1}$, which is in good

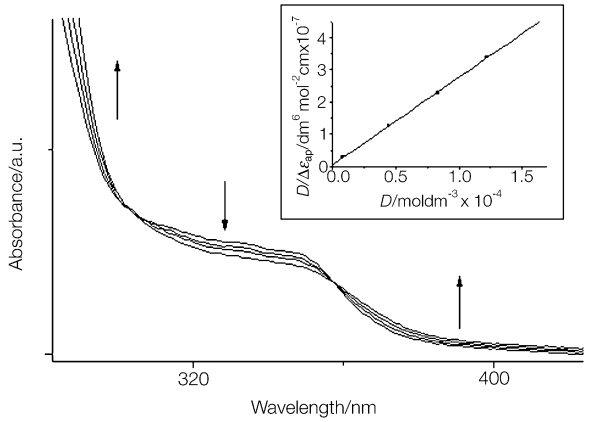

Figure 1. UV/Vis spectra of **1** (100 μM) in Tris buffer solution with increasing ratio of [DNA]/[**1**]: 0.16, 0.44, 0.83, 1.5 at 20 °C. Inset: plot of $D/\Delta\varepsilon_{ap}$ versus D. Absorbance was monitored at 320 nm.

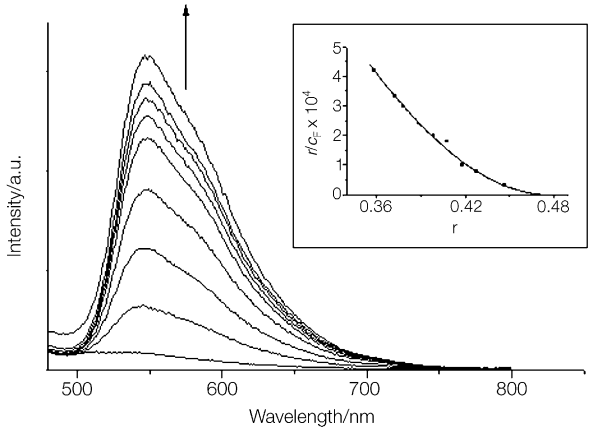

Figure 2. Emission spectral traces of **1** (50 μM) in Tris buffer solution with increasing ratio of [DNA]/[**1**]: 0.54, 2.70, 5.90, 8.54, 11.2, 13.8, 16.4, 18.9, 21.6 at 20 °C. Inset: Scatchard plot for the binding of **1** to ct DNA. The titration was used to generate the solid line in the figure, which was determined by using Equation (3) and a nonlinear least-squares fit for the data points.

agreement with the value of 3.67×10^3 mol^{-1} dm^3 cm^{-1} determined by absorption titration.

The binding of **2** to DNA shows comparable spectral changes, with isosbestic points at 301, 356, and 377 nm (Figure S1, Supporting Information). For the absorption band at 332 nm, 40% hypochromicity and a 12 nm bathochromic shift were observed on addition of calf thymus DNA. According to the literature, substantial hypochromism, extensive broadening, and red shift of absorption band(s) are characteristic of intercalative interaction.[31] With reference to our previous studies,[32] the intrinsic binding constant K for **2** was found to be $(2.3\pm0.3)\times10^4$ mol^{-1} dm^3, which is about 20 times smaller than the K value of $(4.6\pm0.2)\times10^5$ mol^{-1} dm^3 for **1**. In the control experiment with sodium dodecyl sulfate (SDS) instead of calf thymus DNA, no significant difference was observed between the absorption spectra of the platinum(II) complexes in the absence and presence of SDS. This indicates that the absorption spectral changes observed upon addition of double-stranded DNA are not due to electrostatic binding of the cationic platinum(II) complexes to the polyanionic DNA phosphate backbone.

Emission titration: In Tris buffer solution (5 mM Tris, 50 mM NaCl, pH 7.2), the emission intensity of **1** at 547 nm was enhanced on addition of calf thymus DNA (Figure 2) and reached a saturation level (around 18 times the original value) at a [DNA]:[Pt] ratio of 20:1. The concentration of the free complex c_F is determined by Equation (2),[33]

$$c_F = c_T[(I/I_0)-P]/(1-P) \quad (2)$$

where c_T is the total concentration of the free and bound forms of the platinum(II) complex, I and I_0 are the emission intensity in the presence and absence of DNA, respectively, and P is the ratio of the observed emission intensity of the bound complex relative to that of the free complex. The I_0 and P values are obtained by plotting I/I_0 versus 1/[DNA]. The concentration of the bound complex c_B is equal to c_T-c_F. A plot of r/c_F versus r, where $r=c_B$/[DNA], is constructed according to Equation (3),[33]

$$r/c_F = K(1-nr)\{(1-nr)/[1-(n-1)r]\}^{n-1} \quad (3)$$

where n is the size of the binding site in base pairs. The data were fitted by using Equation (3) to obtain the binding parameters. The calculated value is $n=2$, that is, two base pairs of calf thymus DNA are occupied per molecule of **1**. The binding constant K is $(4.9\pm0.3)\times10^5$ mol^{-1} dm^3, which is similar to that of $(4.6\pm0.2)\times10^5$ mol^{-1} dm^3 obtained by absorption titration.

The emission intensity of **2** increased 225-fold on addition of calf-thymus DNA (Figure S2, Supporting Information) and reached a saturation level at [DNA]:[Pt] ratios above 7:1. With reference to our previous work, the binding constant K is $(2.2\pm0.1)\times10^4$ mol^{-1} dm^3 and the n value is 2.4.[32]

Binding to synthetic oligonucleotides: Emission titration experiments of **1** with poly(dA-dT)$_2$ and poly(dG-dC)$_2$ were performed in order to examine sequence selectivity (Figure 3). For poly(dA-dT)$_2$, the emission intensity showed an overall 10-fold enhancement, but no further increase was observed when [DNA]:[Pt] ratios exceeded 15:1. In contrast, no emission enhancement was observed on addition of poly(dG-dC)$_2$ to **1** in Tris buffer solution.

Similar emission titrations of **2** with poly(dA-dT)$_2$ and poly(dG-dC)$_2$ were performed. On addition of poly(dA-dT)$_2$ to **2** in Tris buffer solution, an overall 125-fold increase in emission intensity was observed, and emission intensity reached a maximum at [DNA]:[Pt] ratios above 12:1. Again, no emission enhancement was observed when poly(dG-dC)$_2$ was used. The emission titration results suggest that **1** and **2** preferentially bind to the AT sequence.

The binding of **1** and **2** with poly(dA-dT)$_2$ and poly(dG-dC)$_2$ was further examined by UV/Vis absorption spectroscopy. The spectral changes induced by binding of **1** or **2** to

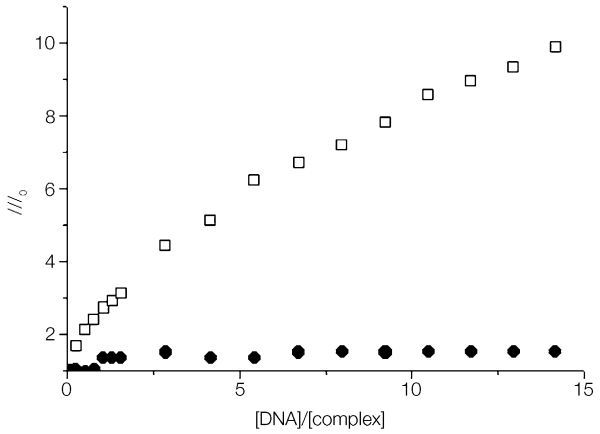

Figure 3. Emission titration curves for **1** with poly(dA-dT)$_2$ (□) and poly(dG-dC)$_2$ (●) in Tris buffer solution. The emission intensities were monitored at 547 nm.

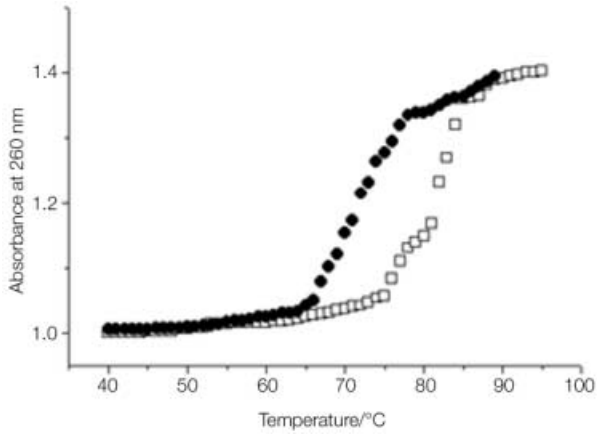

Figure 4. Plots of A/A_0 vs temperature for 33-bp DNA (20 μM) (●) and 33-bp DNA in the presence of **1** (□) with a 1:1 ratio of DNA base pairs to **1** in Tris buffer solution.

calf thymus DNA, poly(dA-dT)$_2$, and poly(dG-dC)$_2$ are similar. Hypochromicity is detected in the 19–40% range, and binding constants K for the reactions of **1** and **2** with poly(dA-dT)$_2$ are around an order of magnitude larger than those for poly(dG-dC)$_2$. The DNA binding data are summarized in Table 1. These results are consistent with the emission titration experiments showing general AT specificity for the binding reactions.

Apart from emission and absorption titrations, UV melting experiments on poly(dA-dT)$_2$ and poly(dG-dC)$_2$ also revealed that **1** and **2** preferentially bind to the AT sequence. In the presence of **1** and **2**, the melting temperature of poly(dA-dT)$_2$ increased from 56 to 75 and 72 °C, respectively. In contrast, less than 1 °C increase in melting temperature was observed for poly(dG-dC)$_2$ under identical reaction conditions (for details of thermodynamic parameters, see Table S1, Supporting Information).

UV melting study: The thermodynamic stability of the metal-bound DNA was studied by measuring the UV/Vis absorption spectra at various temperatures. The melting curves of 33-bp DNA in the absence and presence of **1** are depicted in Figure 4. The melting temperature T_m of the untreated 33-bp DNA was 71 °C, and this increased to 83 and 85 °C upon binding to **1** and **2**, respectively. Treatment of the melting data by using McGhee's equation[34] [Eq. 4] afforded the intrinsic binding constant K_m at the DNA melting temperature.

$$(1/T_m^o - 1/T_m) = (\Delta H_m/R)\ln(1 + K_m L)^{1/n} \quad (4)$$

Here T_m^o and T_m are the respective melting temperatures of the 33-bp DNA in the absence and presence of the platinum(II) complex, ΔH_m is the helix-to-coil transition enthalpy of DNA melting (per bp), R is the gas constant, and L is the concentration of free ligand (approximated as the total ligand concentration at T_m). Values of $\Delta H_m = 7.0 \pm 0.3$ kcal mol^{-1} and $n = 2$ (data obtained from emission titration) were used in the calculation.[35] Equation (4) gave K values of $(1.4 \pm 0.3) \times 10^2$ mol^{-1} dm^3 at 83 °C for **1** and $(1.0 \pm 0.3) \times 10^2$ mol^{-1} dm^3 at 85 °C for **2** (full thermodynamic parameters are listed in Table 2). For **1** (**2**), upon increasing the temperature to 90 °C, spectral hyperchromism at 211 and 260 (216 and 259) nm and isosbestic points at 302 and 366 (310, 356, and 419) nm were found.

Viscosity experiments: The plots of $(\eta/\eta_0)^{1/3}$ versus binding ratio (r_{bound}) for the platinum complex, ethidium bromide (intercalator), and Hoechst 33342 (groove binder) are depicted in Figure 5. The relative viscosity of calf thymus DNA in the presence or absence of the platinum complex was calculated by using Equation (5),

Table 1. Summary of DNA binding data.

Complex	K [mol^{-1} dm^3] at 20 °C			Hypochromicity [%]		
	ct DNA	poly(dA-dT)$_2$	poly(dG-dC)$_2$	ct DNA	poly(dA-dT)$_2$	poly(dG-dC)$_2$
1	$(4.6 \pm 0.2) \times 10^5$	$(1.6 \pm 0.4) \times 10^5$	$(6.8 \pm 0.5) \times 10^4$	27	29	19
2	$(2.3 \pm 0.3) \times 10^4$	$(3.0 \pm 0.6) \times 10^4$	$(4.1 \pm 1.4) \times 10^3$	40	34	33

Table 2. Thermodynamic parameters estimated by absorption titration and DNA melting study

Complex	ΔT_m [°C]	K [mol^{-1} dm^3] at T_m	K [mol^{-1} dm^3] at 20 °C	ΔH [kcal mol^{-1}]	ΔG [kcal mol^{-1}]	ΔS [cal K^{-1} mol^{-1}]
1	12	$1.4 \pm 0.3 \times 10^2$	$4.6 \pm 0.2 \times 10^5$	-26.7 ± 0.4	-7.6 ± 0.1	-65.1 ± 0.3
2	14	$1.0 \pm 0.3 \times 10^2$	$2.3 \pm 0.3 \times 10^4$	-17.4 ± 0.2	-5.8 ± 0.2	-39.6 ± 0.3

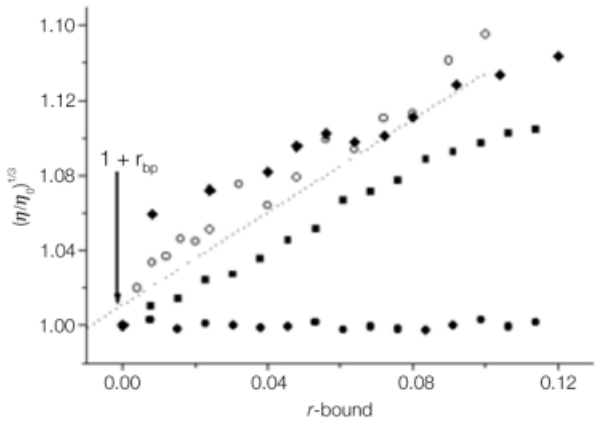

Figure 5. Relative specific viscosity of ct DNA in the presence of ethidium bromide (◆), Hoechst 33342 (●), **1** (■) and **2** (○) as a function of the binding ratio.

$$\eta = (t - t_0)/t_0 \quad (5)$$

where t is the flow time of the DNA-containing solution, and t_0 is the flow time of buffer solution alone. According to Cohen and Eisenberg,[36] the relationship between the relative solution viscosity η/η_0 and contour length L/L_0 is given by $L/L_0 = (\eta/\eta_0)^{1/3}$, where L_0 and η_0 denote the apparent molecular length and solution viscosity in the absence of the metal complex. An increase in relative viscosity reflects an increase in apparent molecular length. Insertion of organic or metal/organic molecule(s) between the stacked bases within a linear host duplex would lead to lengthening of the DNA duplex. Thus, the observed increase in viscosity of the DNA solution on addition of **1** or **2** (Figure 5) is consistent with an intercalative binding mode.

Gel mobility shift assay: The results of gel electrophoresis on a 100-bp DNA ladder (Amersham Pharmacia biotech) in the absence and presence of **1**, **2**, ethidium bromide, and Hoechst 33342 are depicted in Figure 6. A single band observed in lane A corresponds to the 100-bp DNA ladder. In the presence of **1**, a slight decrease in DNA mobility in a dosage-dependent manner was observed. The gel mobility shift assay for **2** was reported in the literature:[32] significantly reduced DNA mobility in a dosage-dependent manner was found, and the extent of the mobility reduction was comparable to that detected when the DNA solution was treated with ethidium bromide.[37]

Restriction endonuclease fragmentation assay: The results of electrophoresis of restriction enzyme digestion of pDR2 in the absence and presence of **1** are depicted in Figure 7. Two bands corresponding to supercoiled and nicked DNA were observed for the undigested DNA (lane B). After ApaI digestion of pDR2, three bands corresponding to DNA fragments with 8, 5, and 2 kbp were obtained and resolved by agarose gel electrophorsis (lane C). In the presence of the classical intercalator ethidium bromide (4 μM), the minor groove binder Hoechst 33342 (200 μM), or the intrastrand cross-linker cisplatin (200 μM), DNA digestion was incomplete, and bands attributable to the whole plasmid

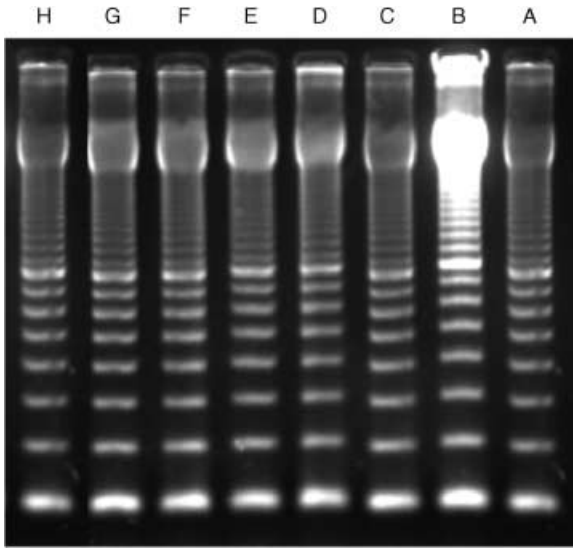

Figure 6. Gel electrophoresis of a 100-bp DNA ladder in 2% (w/v) agarose gel showing the mobility of DNA. Lanes A and H are the 100-bp DNA. Lanes B and C are the 100-bp DNA in the presence of DNA-interacting molecules: ethidium bromide (152 μM, lane B) and Hoechst 33342 (152 μM, lane C). Lanes D–G are the 100-bp DNA in the presence of **1** at 152 μM (lane D), 76 μM (lane E), 30 μM (lane F), and 15.2 μM (lane G).

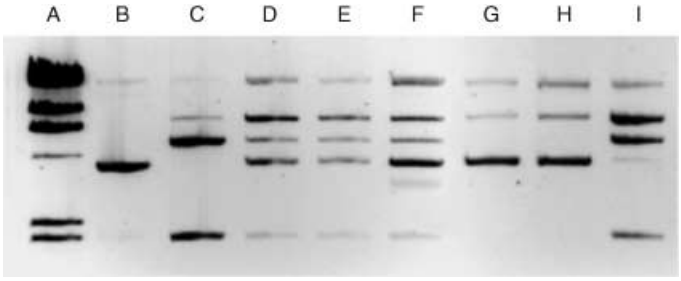

Figure 7. Inhibition of restriction endonuclease ApaI cutting sites by various small molecules. Lane A is a size marker. Lanes B and C are undigested and ApaI (1 unit/μL) digestion products of pDR2 DNA (10.7 kbp, 21 nM bp^{-1}), respectively. Lanes D–F are the digestion products of pDR2 DNA in the presence of DNA-interacting molecules: ethidium bromide (4 μM, lane D), Hoechst 33342 (200 μM; lane E), cisplatin (200 μM; lane F). Lanes G–I are the digestion products of pDR2 DNA in the presence of **1** at 200 μM (lane G), 20 μM (lane H), and 2 μM (lane I).

plus fragments were observed. At a high concentration of **1** (200 μM), complete inhibition of ApaI digestion was found, while partially inhibited cleavage was observed at a lower concentration (2 μM). The results indicate that restriction enzymatic digestion of plasmid was stopped or retarded by those molecules that interact with DNA through intercalation, groove binding, and/or cross-linkage. Interestingly, the same result was obtained for **2**.[32] Previous work by Neidle et al.showed that enzymatic DNA cleavage is inhibited when the local conformation of the enzyme binding site or the restriction site is altered due to metal complex binding.[38] Thus, the results of restriction endonuclease fragmentation assay indicate that **1** and **2**, like other intercalators, groove binders, and covalent cross-linkers, can alter the conformation of DNA.[39]

NMR titration of d(CAATCCGGATTG)$_2$ with 1 and 2: The NMR spectra of d(CAATCCGGATTG)$_2$ at [**1**]/[d(CAATCCGGATTG)$_2$] ratios of 2.0, 1.5, 0.5, and 0 are shown in Figure 8. Addition of **1** induces small changes in the chemical shifts of the major-groove purine H_8 and pyrimidine H_6 resonances, while the minor groove A_2H_2 resonance shows a large downfield shift. The C_1 and G_{12} resonances show slightly larger downfield shifts than the other major-groove protons (Table 3). This is consistent with binding of **1** to the minor groove near the A_2 residue of d(CAATCCGGATTG)$_2$.[40]

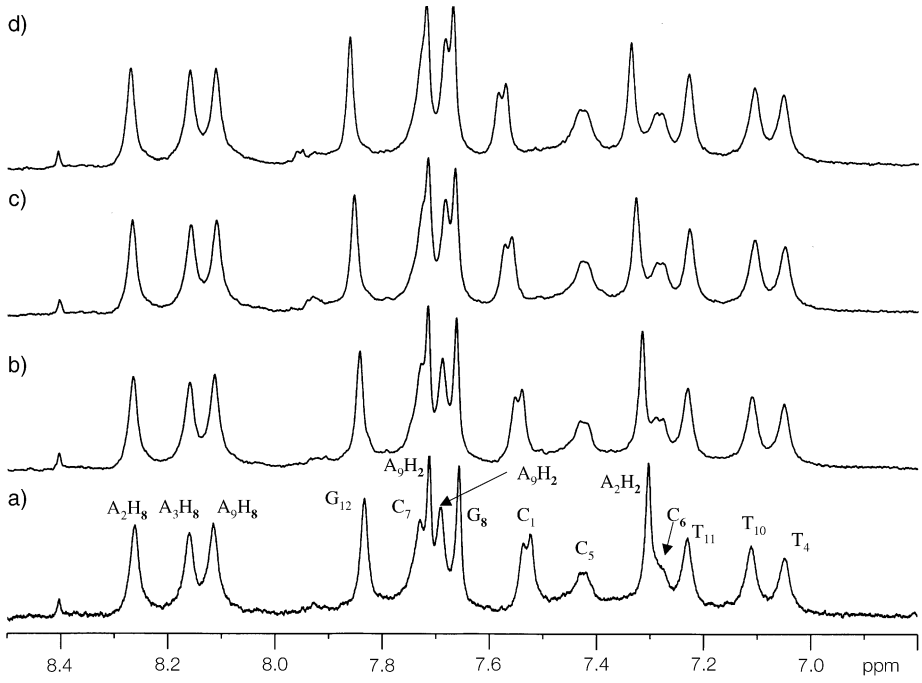

Figure 8. ^{1}H NMR spectra (500 MHz, D_2O) of the aromatic base protons of d(CAATCCGGATTG)$_2$ (1.0 mM) at [**1**]/[d(CAATCCGGATTG)$_2$] ratios of a) 0, b) 0.5, c) 1.5, and d) 2.0.

The NMR spectra of d(CAATCCGGATTG)$_2$ at [**2**]/[d(CAATCCGGATTG)$_2$] ratios of 2.0, 1.0, and 0 are shown in Figure S3 (Supporting Information). Addition of **2** causes large changes in the chemical shifts of the major- and minor-groove protons (see Table 4), with A_9H_8 and T_{10} proton signals displaying the largest upfield shifts (0.09 and 0.061 ppm, respectively). In general, the DNA spectrum broadens and shifts upfield in the presence of **2**.

Cytotoxicity test (MTT Assay): The cytotoxicities of **1** and **2** against the five human carcinoma cell lines KB-3–1, KB-V-1, CNE-3, HepG2, CNE1, and normal CCD-19 Lu were studied (Table 5). The cytotoxicity was measured by MTT assay, and the IC_{50} values were determined from the dose-dependence of surviving cells after exposure to the platinum(II) complexes for 48 h (Figure 9). The antitumor activities under our experimental conditions (final concentration $\leq$4% DMSO) are in the order: **1** $\approx$ cisplatin $>$ 4-dpt $>$ **2**. Thus, **1** is more cytotoxic than the free ligand 4-dpt and exhibits cytotoxicity that is comparable to that of cisplatin. When cisplatin was dissolved in H_2O and mixed with the growth medium, the cytotoxicity was 2–5 times higher than that containing DMSO (final concentration $\leq$4% DMSO). Against CNE-3, **1** is almost 10 times more effective than **2**, while it is 20 times more toxic than **2** for KB-3-1. Complex **1** remains potent against multidrug- and cisplatin-resistant KB-V-1 and CNE1 cell lines; the resistance ratios are 1.6 and 1.5 respectively. Importantly, **1** is almost an order of magnitude less toxic to the CCD-19Lu normal cell line.

Table 3. ^{1}H NMR chemical shifts [ppm] of d(CAATCCGGATTG)$_2$ and chemical shift differences[a] (in parentheses) induced by addition of **1** at a [**1**]/[d(CAATCCGGATTG)$_2$] ratio of 2.

	H_8/H_6	AH_2
C_1	7.53065 (**0.035**)	
A_2	8.2611 (0.006)	7.3032 (**0.024**)
A_3	8.1600 (−0.002)	7.6911 (−0.009)
T_4	7.0493 (−0.001)	
C_5	7.4256 (−0.0002)	
C_6	7.2788 (0.004)	
G_7	7.7301 (−0.004)	
G_8	7.6570 (0.008)	
A_9	8.1150 (−0.005)	7.7124 (0.0025)
T_{10}	7.1120 (−0.007)	
T_{11}	7.2301 (−0.0035)	
G_{12}	7.8336 (**0.02**)	

[a] Significant chemical shift differences (0.01 ppm or more) are shown in bold face. Positive numbers indicate a downfield shift.

Table 4. ^{1}H NMR chemical shifts [ppm] of d(CAATCCGGATTG)$_2$ and chemical shift differences (in parentheses) induced by addition of **2** at a [**2**]/[d(CAATCCGGATTG)$_2$] ratio of 2.

	H_8/H_6	AH_2
C_1	7.5701 (−0.0311)	
A_2	8.2826 (−**0.0549**)	7.3159 (−0.0394)
A_3	8.1719 (−**0.05025**)	7.7000 (−0.0073)
T_4	7.0574 (−0.0074)	
C_5	7.4311 (−0.0037)	
C_6	7.2893 (−0.0128)	
G_7	7.7402 (−0.0475)	
G_8	7.6735 (−0.0403)	
A_9	8.1207 (−**0.0924**)	7.7210 (−0.0283)
T_{10}	7.1256 (−**0.0612**)	
T_{11}	7.2454 (−**0.0521**)	
G_{12}	7.8546 (−**0.0573**)	

[a] Significant chemical shift differences (0.05 ppm or more) are shown in bold face.

Table 5. Cytotoxicities of **1**, **2**, cisplatin, and 4-dpt in human carcinoma KB-3-1, multidrug-resistant subclone KB-V-1, CNE-3, HepG2, CNE1, and CCD-19 Lu (normal) cells.

Complex	IC_{50} [μM]					
	KB-3-1	KB-V-1	CNE-3	HepG2	CNE1	CCD-19 Lu
1[a]	18.4±0.9	28.8±1.9	12.9±1.1	54.6±2.8	18.1±2.1	176±1.7
2[a]	388±1.2	654±2.4	135±0.4	45.0±1.3	n.d.[c]	n.d.[c]
cisplatin[a]	22.1±3.6	39.1±1.7	10.5±2.6	10.5±0.5	n.d.[c]	129±0.9
4-dpt[a]	72.1±3.9	79.6±4.1	68.2±2.3	84.7±1.6	n.d.[c]	n.d.[c]
cisplatin[b]	5.4±2.1	8.5±1.9	6.4±1.5	6.1±2.7	n.d.[c]	n.d.[c]

[a] Compound was dissolved in DMSO and mixed with the growth medium (final concentration ≤4% DMSO). [b] Compound was dissolved in H_2O and mixed with the growth medium. [c] Not determined.

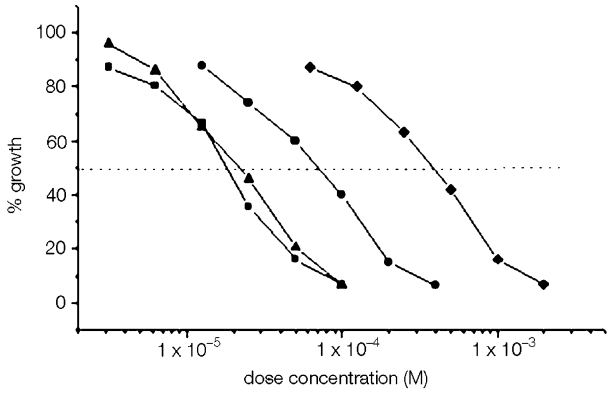

Figure 9. Plots of percentage growth versus dose concentration of KB-3-1 cells in the presence of **1** (■), cisplatin (▲), 4-dpt (●), and **2** (◆).

DNA fragmentation assay: The results of gel electrophoresis of the DNA extracted from KB-3-1 cells after different treatments are depicted in Figure 10. Treatment of KB-3-1 cells with **1** at IC_{50} concentration resulted in a "DNA ladder" (fragmentation of genomic DNA in nucleosome units) indicative of apoptosis. The result is the same as that found for apoptosis induced by UV light.

Fluorescence and confocal microscopy: On the basis of cell morphology and cell-membrane integrity, normal, necrotic, and apoptotic cells can be distinguished by laser confocal microscopy. The types of cell death induced by **1** are depicted in Figure 11.

In the absence of cisplatin or **1**, the nucleus of a living cell was stained as a bright green spot. However, in their presence, green apoptotic cells with apoptotic bodies and red necrotic cells were observed. The results show that **1**, like cisplatin, can induce apoptosis in KB-3-1 cell line.

Flow cytometric analysis: Distributions of cell deaths for **1** are depicted in Figure 12. The result shows that **1** induced 51.8±2.3% apoptosis selectively leading to cancer cell death, and only 4.6±0.2% necrosis was detected. However, **2** induced apoptosis and necrosis of 45.4±0.9 and 18.7±0.7%, respectively. The cell-death distributions for **1** and **2** are summarized in Figure 13.

Discussion

Complexes **1** and **2** resemble the classic metallointercalator $[Pt(terpy)Cl]^+$ in their square-planar geometry and monocationic nature. However, complex **1** features a distinctive pyridyl ligand with the capability to engage in hydrogen bonding interactions. The present results indicate that the binding modes of **1** and **2** to DNA are different. As observed by UV/Vis spectroscopy, binding of **1** to DNA causes no shift in its absorption maximum at 320 nm, but a decrease in peak intensity (27% hypochromicity) and a binding constant K of $4.6\times10^5\ mol^{-1}\,dm^3$ are observed. For **2**, 40% hypochromicity and a 12 nm bathochromic shift of the absorption maximum at 332 nm are found. The K value for **2** is $2.3\times10^4\ mol^{-1}\,dm^3$, which is comparable to that for related platinum(II) complexes such as $[Pt(terpy)py]^{2+}$ ($3.5\times10^4\ mol^{-1}\,dm^3$),[41] $[(phen)Pt(en)]^{2+}$ ($5\times10^4\ mol^{-1}\,dm^3$),[4] $[(bpy)Pt(en)]^{2+}$ ($1\times10^4\ mol^{-1}\,dm^3$),[42] $[Pt(5,5'\text{-}Me_2bpy)(4\text{-}ampy)_2]^{2+}$ (5,5′-Me_2bpy = 5,5′-dimethyl-2,2′-bipyridine, 4-ampy = 4-aminopyridine; $1.8\times10^4\ mol^{-1}\,dm^3$),[43] $[Pt_2(CNN)_2(\mu\text{-}dppm)]^{2+}$ (dppm = bis(diphenylphosphanyl)-methane; $4.4\times10^4\ mol^{-1}\,dm^3$)[22] and $[Pt(dppz)(t\text{NC})]^+$ (dppz = dipyrido[3,2-*a*:2′,3′-*c*]phenazine, H*t*NC = 4-*tert*-butyl-2-phenylpyridine; $1.3\times10^4\ mol^{-1}\,dm^3$),[7] all of which have been shown or proposed to interact with DNA by intercala-

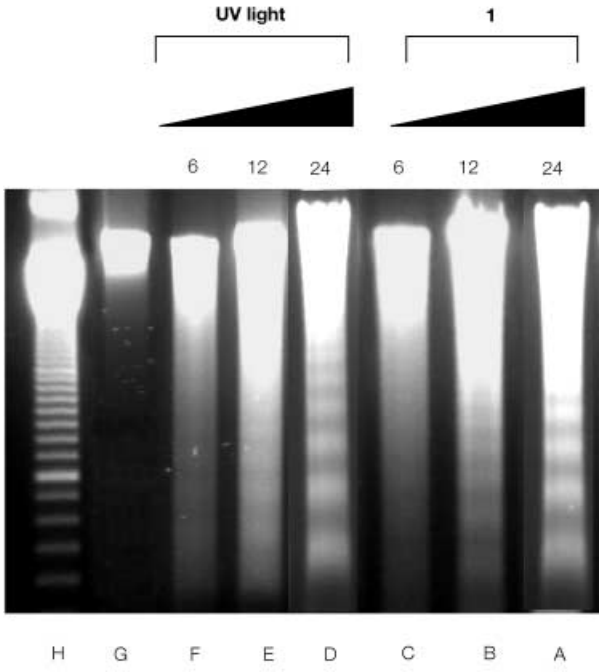

Figure 10. Agarose gel electrophoresis of DNA extracted from KB-3-1 cells subjected to different treatments: Incubation in the presence of **1** (IC_{50}) for 24, 12, and 6 h incubation time, respectively (lanes A–C), 60 mJ cm^{-2} UV light for 24, 12, and 6 h incubation time, respectively (lanes D–F), and no treatment (lane G). Lane H is a DNA marker.

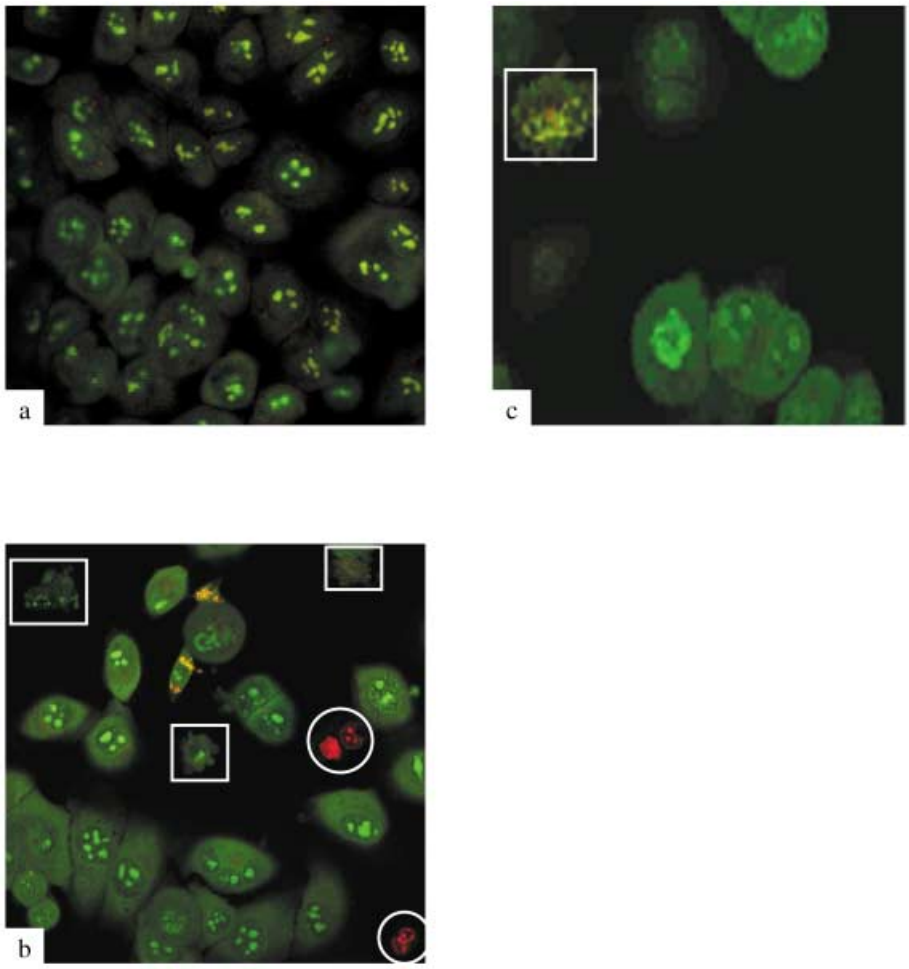

Figure 11. KB-3-1 cells were stained by AO/EB and observed by laser scanning confocal microscopy. KB-3-1 cells in the absence (a) and presence of cisplatin (22 μM, b), **1** (18 μM, c) incubated at 37 °C and 5% CO_2/95% air in a humidified incubator for 72 h. Cells in circles and rectangles are necrotic and apoptotic cells, respectively.

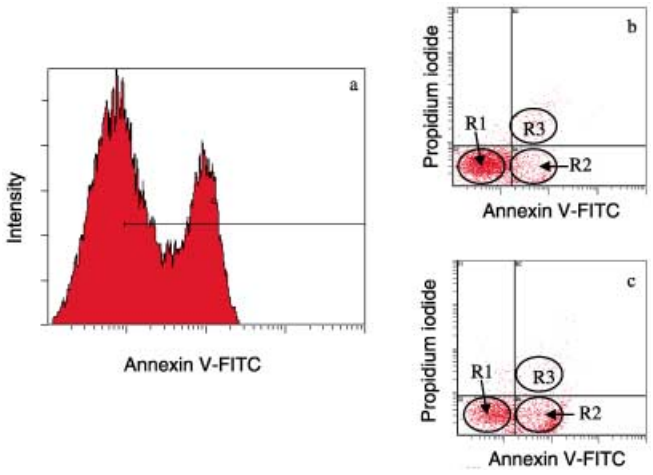

Figure 12. FACS analysis of apoptotic HeLa cells by Annexin-V-FLUOS and propidium iodide. a) Single-parameter Annexin-V-Fluos (cultivation for 12 h in the presence of **1**), b) dual-parameter (cultivation for 12 h in the absence of **1**), c) dual-parameter (cultivation for 12 h in the presence of **1**); cluster R1 = living cells, R2 = apoptotic cells, and R3 = necrotic cells.

tion. Thus the K value, hypochromicity, and bathochromic shift in absorption maximum are consistent with **2** binding to DNA in an intercalative mode. The K value for **1** is 23 times larger than that of **2**. This finding, together with the low hypochromicity and lack of spectral bathochromic shift for the reaction between **1** and DNA, suggests that intercalation is not the major mode of binding. The hydrogen-bonding functionality of the 4-dpt ligand in **1** should allow this complex to act as a groove binder.[44] Indeed, the ^{1}H NMR study of the reaction of **1** with d(CAATCCGGATTG)$_2$ indicates the involvement of hydrogen bonding in the binding process. We suggest that the binding of **1** to DNA entails hydrogen bonding of the coordinated 4-dpt ligand with the groove walls. Moreover, the K value of **1** is comparable to that for free bithiazole of bleomycin (1×10^5 mol^{-1} dm^3), which is known to bind to DNA by both intercalation and groove binding.[45]

Binding of both **1** and **2** to DNA led to enhancement of the ^{3}MLCT emission originating from the triplet [Pt→π*(CNN)] excited state. Here, the environmental effects imposed by the 4-dpt or py ligand on the emissive excited state, which primarily involves the CNN ligand, should be minimal. In previous studies, Barton et al. attributed intensity enhancements and increased lifetimes

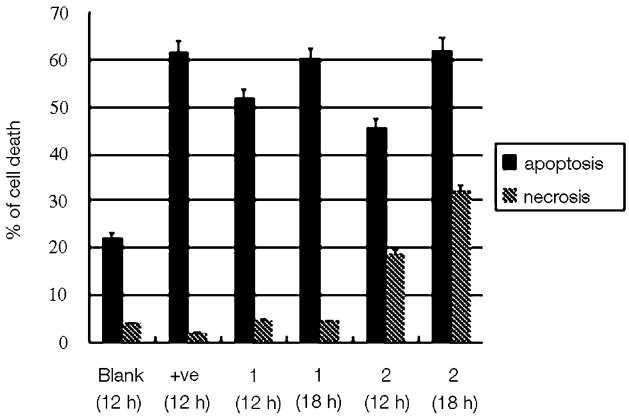

Figure 13. Distributions of cell deaths for **1**, **2**, and positive control (*Staurosporin streptomyces*) at 12 or 18 h incubation time.

for the ^{3}MLCT emissions of octahedral $[Ru(diimine)_3]^{2+}$ complexes to their decreased mobility on intercalation between the base pairs of calf thymus DNA.[46,47] A similar reasoning could be invoked to rationalize enhancement of the ^{3}MLCT emission of **1** in the presence of calf thymus DNA. Intercalative binding of the [Pt(CNN)] moiety of **1** to duplex DNA would result in protection of the hydrophobic [Pt(CNN)] unit from aqueous buffer solution, and nonradiative decay of the excited state by complex–solvent interaction is thus suppressed. However, the maximum enhancement in emission intensity is only 18-fold, which is much smaller than the 225-fold observed for binding of **2** to calf thymus DNA, despite the fact that the latter has a smaller K value. We propose that **1** binds to DNA by hydrogen-bonding (presumably major) and intercalative modes, and the hydrogen bonding contributes significantly to the magnitude of the binding constant but exerts a minimal effect on the ^{3}MLCT emission.

Ultraviolet melting, viscosity, gel mobility shift assay, and high-resolution NMR experiments were performed to elucidate the DNA-binding mode(s) of **1** and **2**. The binding reactions are exothermic according to their negative ΔH values. Because ΔH values are known to correlate with the number of hydrogen bonds to DNA and the number of van der Waals contacts,[48] we can compare the ΔH values of **1** and **2** with those of previously reported groove binders that preferentially and peripherally bind the AT sequence. For example, Distamycin A forms four NH hydrogen bonds ($\Delta H = -18.5$ kcal mol^{-1}),[49] Netropsin forms three ($\Delta H = -9.2$ kcal mol^{-1}),[50] Hoechst 33258 forms two ($\Delta H = -6.2$ kcal mol^{-1}),[18] and DAPI forms only one ($\Delta H = -4.5$ kcal mol^{-1}).[51] Based on the data listed in Table 2, ΔH of the reaction of **1** with duplex DNA (-26.7 kcal mol^{-1}) is significantly more exothermic than that of the corresponding reaction with ethidium bromide (-10 kcal mol^{-1}) or Netropsin (-9.2 kcal mol^{-1}).[52] Hence, **1** behaves neither like a pure intercalator nor a distinct groove binder. An intercalator would significantly increase the hydrodynamic length of sonicated DNA, while a groove binder has no effect on the solution viscosity of DNA.[53] For **1**, a competing nonintercalative binding mode could reduce the extent of helix lengthening. This may explain the observed increase in DNA length on reaction with **1**, which falls short of the theoretical value of $1 + r_{bp}$ predicted by the classical model for intercalation into a rodlike nucleic acid.[36]

The results of gel mobility shift assay revealed that, like ethidium bromide,[37] the 100-bp DNA ladder was lengthened by **2**, and DNA mobility was significantly reduced in a dosage-dependent manner. The electrophoretic pattern showed that the DNA mobility was only slightly affected by increasing concentrations of **1**. This is consistent with groove binding as the major binding mode of **1** towards the 100-bp DNA. Direct evidence for the involvement of hydrogen bonding in the reaction of **1** with dodecanucleotides was obtained in ^{1}H NMR experiments. Addition of **2** to $d(CAATCCGGATTG)_2$ induced substantial changes in the chemical shifts of the major- and minor-groove protons; broadening of the spectrum and upfield shifts are characteristic of an intercalative binding mode. However, addition of **1** to $d(CAATCCGGATTG)_2$ was found to cause a relatively large downfield shift (0.024 ppm) for the minor-groove A_2H_2 reasonance, and there were only relatively small chemical shift differences (± 0.008 ppm) for all major-groove proton resonances. Hence, the ^{1}H NMR data are indicative of binding of **1** to the minor groove of DNA. By taking all the results described in previous sections into consideration, we propose that mixed DNA binding modes are exhibited by **1** in which the Pt(CNN) moiety intercalates into the helical stack while the 4-dpt ligand protrudes into the minor groove, as schematically depicted in Figure 14.

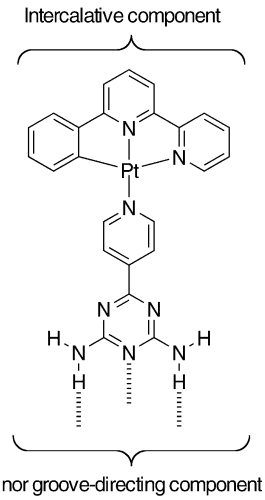

Figure 14. Schematic representation of the DNA-binding components of **1**.

AT sequence specificity: Overall 10- and 125-fold increases in emission intensity were observed on additon of poly(dA-dT)$_2$ to **1** and **2**, respectively. In contrast, no emission enhancement was observed when poly(dG-dC)$_2$ was used as substrate, and the binding constants K for the reactions of **1** and **2** with poly(dA-dT)$_2$ are around an order of magnitude larger than those with poly(dG-dC)$_2$. These findings clearly indicate their specificity for AT base-pair binding. In the AT-rich regions of the minor groove, **1** is stabilized by van der Waals interactions and by hydrogen bonding to the N3 atoms of adenine and/or O2 atoms of thymine residues. Additionally, more favorable electrostatic interaction would be achieved in the minor groove of AT sequences, which have higher negative electrostatic potential than GC sequences. Similar observations were made for other minor-groove binders, such as Hoechst 33258.[54–57]

Cytotoxicity: As depicted in Table 5, there is no significant variation in the cytotoxicity of **1** and cisplatin towards different cell lines under our experimental conditions (final concentration $\leq 4\%$ DMSO). Against CNE-3, **1** is almost 10 times more effective than **2**, while it is 20 times more toxic than **2** for KB-3-1,; this illustrates the value of hydrogen-bonding motifs in the pyridyl ligand for the design of platinum-based antitumor agents. Note that the 4-dpt substrate alone exhibits poor cytotoxicity relative to **1**. Importantly, **1**

is almost an order of magnitude less toxic to the CCD-19 Lu normal cell line.

One of the major problems in cancer chemotherapy is the development of tumors that are resistant to drug treatment.[58] The mechanism leading to multidrug resistance is overexpression of the mdr1 gene product, a 170 kDa membrane P-glycoprotein which is an ATP-driven efflux pump of xenobiotics.[58,59] Here, we studied the effects of **1** on the multidrug-resistant phenotype in human KB carcinoma cells. The cytotoxicity results based on the KB-3-1 and KB-V-1 cell lines show that the IC_{50} values of **1** are nearly the same, and the resistance ratio is 1.6 (KB-V-1). Thus, although the KB-V-1 cell line is resistant to anticancer drugs such as colchicine, vinblastin, and doxorubicin, its multidrug-resistance mechanism does not function on **1**. Moreover, **1** remains potent against the CNE1 cell line, which is resistant to existing clinical platinum-based drugs (e.g., cisplatin).

There are two types of cell death, namely necrosis ("accidental") and apoptosis ("programmed").[60,61] Necrotic cells undergo cell lysis and lose their membrane integrity, and severe inflammation is induced.[62] However, apoptotic cells are transformed into small, membrane-bound vesicles (apoptotic bodies), which are engulfed by macrophages in vivo, and no inflammatory response is found.[63,64] Hence, induction of apoptosis is important in cancer chemotherapy. Most of the anticancer drugs in current use have been shown to induce apoptosis in susceptible cells.[65] In this regard, we found that **1** induces a high degree of apoptosis, as established by analysis by confocal microscopy and DNA fragmentation assay, and through quantitative measurements by flow cytometric analysis.

Conclusion

[Pt(CNN)(4-dpt)]PF_6 (**1**), which bears a triple hydrogen-bonding motif, binds to the DNA double helix with a binding constant of $(4.64\pm0.2)\times10^5\,mol^{-1}\,dm^3$ at 20 °C. The spectral data support a specific binding mode at the AT sequences of DNA. The thermodynamic properties of the binding reaction were determined by absorption titration and UV melting studies. The electronic interaction between the Pt chromophore and DNA bases and the structural and conformational changes within the DNA helix were examined by various spectroscopic, electrophoretic, and hydrodynamic methods. The binding mode for [Pt(CNN)(py)]PF_6 (**2**), which bears no hydrogen bonding motif for DNA, was found to be intercalation. For **1**, both intercalation and minor-groove binding modes were demonstrated. Complex **1** is cytotoxic against a number of carcinoma cell lines, including KB-3-1, CNE-3, and HepG2, and the activities are comparable to those of cisplatin under our experimental condition (final concentration $\leq4\%$ DMSO). Moreover, **1** remains potent against multidrug- and cisplatin-resistant KB-V-1 and CNE1 cell lines, for which the resistance ratios are 1.6 and 1.5, respectively. Significantly, **1** is almost an order of magnitude less toxic to the normal cell line CCD-19 Lu ($IC_{50}=176\pm1.7\,\mu M$). By examining the qualitative and quantitative cytotoxic effect of **1** on cancer cells, it was revealed that **1** selectively induced apoptosis leading to cancer cell death, and necrosis was below 5%.

Experimental Section

Calf thymus DNA (ct DNA) was purchased from Sigma Chemical Co. Ltd. and purified by the literature method.[66] Poly(dG-dC)$_2$ and poly(dA-dT)$_2$ (Sigma Chemical Co Ltd.) were used as received without further purification. The dodecanucleotide d(CAATCCGGATTG)$_2$ was obtained from GENSET Singapore Biotechnology Ltd. The DNA concentration per base pair was determined by UV/Vis absorption spectroscopy by using the following molar extinction coefficients ($M^{-1}cm^{-1}$ bp) at the indicated wavelengths: ct DNA, $\varepsilon_{260}=13200$; d(CAATCCGGATTG)$_2$, $\varepsilon_{260}=13200$; poly(dG-dC)$_2$, $\varepsilon_{254}=16800$; poly(dA-dT)$_2$, $\varepsilon_{260}=12000$.[67] Two complementary oligonucleotides—5′-GCTCCCCTTTCTTGCGGA-GATTCTCTTCCTCTG and 5′-CAGAGGAAGAGAATCTCCGCAA-GAAAGGGGAGC—were obtained from DNAgency (Malvern, USA) and annealed to give a double-stranded 33-bp DNA. The purity of the 33-bp DNA was checked by electrophoresis in a 20% polyacrylamide gel. A plasmid DNA, pDR2 (10.7 kb), was purchased from Clontech Laboratories Inc. (Palo Alto, USA). Unless otherwise stated, DNA-binding experiments were performed in aerated Tris buffer solutions (5 mM Tris, 50 mM NaCl, pH 7.2) at 20 °C. 2,4-Diamino-6-(4-pyridyl)-1,3,5-triazine (4-dpt),[25] 6-phenyl-2,2′-bipyridine (HCNN),[68] [Pt(CNN)Cl],[69] and [Pt(CNN)(py)]PF_6 (**2**)[28] were prepared according to reported procedures.

X-ray structure determination: The 4-dpt ligand and [Pt(CNN)(py)]CF_3SO_3 were characterized by X-ray crystallography. Crystal parameters and details of collection and refinement data are listed in Table S2 (Supporting Information). Perspective views of the 4-dpt molecule and [Pt(CNN)(py)]$^+$ cation are depicted in Figures S4 and S5 (Supporting Information), respectively. X-ray diffraction data were collected on a MAR diffractometer with a 300 mm image plate detector at 301 K using graphite-monochromatized $Mo_{K\alpha}$ radiation ($\lambda=0.71073$ Å). The structures were refined by full-matrix least-squares methods against F_o^2 using the program SHELXL-97.[70] CCDC 206062 (**2**) and CCDC-206061 (4-dpt) contain the supplementary crystallographic data for this paper. These data can be obtained free of charge via www.ccdc.cam.ac.uk/conts/retrieving.html (or from the Cambridge Crystallographic Data Centre, 12 Union Road, Cambridge CB21EZ, UK; fax: (+44) 1223-336-033; or deposit@ccdc.cam.uk).

Spectroscopic titrations and lifetime measurements: Absorption and emission spectra were recorded on a Perkin-Elmer Lambda 19 UV/Vis and a SPEX Fluorolog-2 Model F11 fluorescence spectrophotometer, respectively. Emission lifetimes were measured with a Quanta Ray DCR-3 pulsed Nd:YAG laser system (pulse output 355 nm, 8 ns). The emission signals were detected by a Hamamatsu R928 photomultiplier tube and recorded on a Tektronix model 2430 digital oscilloscope. Estimated error limits: λ (±1 nm); τ ($\pm10\%$); ϕ ($\pm10\%$).

UV melting study: UV melting studies on 33-bp DNA were performed with a Perkin-Elmer Lambda 19 UV/Vis spectrophotometer equipped with a Peltier temperature programmer PTP-6. Solutions of DNA in the absence and presence of the platinum complex (DNA base pair:metal complex = 1:1) were prepared in a Tris buffer solution. The temperature of solution was increased at a rate of 1 °C min^{-1}, and the absorbance at 260 nm was continuously monitored. The T_m values were determined graphically from the plot of absorbance versus temperature.

Viscosity experiments: Viscosity experiments were performed on a Cannon-Manning Semi-Micro Viscometer immersed in a thermostatically controlled water bath maintained at 27 °C.[36,53,71] Titrations were performed by addition of small volumse of concentrated stock solutions of metal complex to a solution of calf thymus DNA in BPE buffer (6 mM Na_2HPO_4, 2 mM NaH_2PO_4, and 1 mM Na_2EDTA, pH 7.0) in the viscometer. Mixing of the solutions in the viscometer was achieved by bubbling with nitrogen gas. The concentration of DNA was approximately 1 mM (in base pairs).

Gel mobility shift assay: A 100-bp DNA ladder (Amersham Pharmacia biotech, 15.2 $\mu M\,bp^{-1}$) was mixed with ethidium bromide, Hoechst 33342

trihydrochloride trihydrate, and the platinum complex at various DNA:Pt ratios (1:10, 1:5, 1:2, and 1:1). The mixture was analyzed by gel electrophoresis (Pharmacia Biotech GNA-200 submarine unit with Power Pac 300 power supply, Bio-Rad) with a 2% (w/v) agarose gel and 1× Tris-acetate-EDTA (TAE) buffer.

Restriction endonuclease fragmentation assay: Digestion of plasmid pDR2 (10.7 kb) with restriction enzyme ApaI (Boehringer Mannheim) was performed by mixing the DNA (21 nM bp^{-1}) in 1× SuRE/Cut Buffer A with ApaI (1 unit/μL), followed by incubation at 37°C for 1 h.[72] A mixture of ethidium bromide (4 μM), Hoechst 33342 (200 μM), *cis*-$[PtCl_2(NH_3)_2]$ (cisplatin; 200 μM), **1** or **2** (0.2–200 μM) and a plasmid pDR2 (10.7 kbp, 21 nM bp^{-1}) in digestion buffer was first incubated at room temperature for 5 min before addition of restriction enzyme (1 unit/μL). Two controls of pDR2 in the absence and presence of restriction enzyme in digestion buffer were prepared. All solutions were incubated at 37°C for 1 h; after digestion with the restriction enzyme, the samples were analyzed by agarose gel electrophoresis.

NMR experiments: All ^{1}H NMR experiments were performed with a Bruker DRX500 spectrometer at 298 K. Typical acquisition conditions for a ^{1}H NMR spectrum were 45° pulse length, 2.0 s relaxation delay (4 s for determination of formation constants), 16000 data points and 16–32 transients. The dodecanucleotide $d(CAATCCGGATTG)_2$ was dissolved in phosphate buffer (0.7 mL, 10 mM, pH 7.0) containing NaCl (20 mM) and EDTA (0.1 mM), and a trace of DSS was added as internal reference for reporting chemical shifts. For experiments in D_2O, the sample was repeatedly freeze-dried from D_2O and finally made up in 99.96% D_2O. Aliquots of stock solutions of **1** were titrated directly to the DNA solution in an NMR tube. The spectra were then processed by using an exponential function with a line-broadening coefficient of 0.3 Hz.

Cytotoxicity test (3-(4,5-dimethylthiazol-2-yl)-2,5-tetrazolium bromide (MTT) assay): The parental epidermal carcinoma KB-3-1 cell line and the multidrug-resistant KB-V-1 cell line derived from KB-3-1 cells by a series of stepwise selections in anticancer agent (vinblastin) were provided by Dr. Michael Gottesman of the National Institute of Health, Bethesda.[58,59] KB-V-1 cells were maintained in the presence of 1 μg mL^{-1} vinblastin. CNE-3 (nasopharyngeal)[73] and HepG2 (hepatocellular)[74] cell lines were provided by Prof. W. F. Fong of City University of Hong Kong, Hong Kong SAR. The cisplatin-resistant CNE1 cell line was derived from poorly differentiated NPC in Chinese patients.[75] CCD-19 Lu (normal lung fibroblast) was obtained from American Type Culture Collection. Cell Proliferation Kit I (MTT) from Roche was used for cytotoxicity evaluation. Briefly, cells were seeded in a 96-well flat-bottomed microplate at 20000 cells per well in 150 μL of growth medium solution [10% fetal calf serum (FCS, Gibco), 1% Sigma A-7292 Antibiotic and Antimycotic Solution in minimal essential medium (MEM-Eagle, Sigma)]. Complexes **1**–**3** and cisplatin (positive control) were dissolved in DMSO and mixed with the growth medium (final concentration $\leq$4% DMSO). Serial dilution of each complex was added to each well (the complex-containing media were drawn and added to another set of wells and such processes were repeated to provide a twofold dilution series). The microplate was incubated for 48 h at 37°C, 5% CO_2, 95% air in a humidified incubator. After incubation, 10 μL MTT reagent (5 mg mL^{-1}) was added to each well. The microplate was then re-incubated at 37°C in 5% CO_2 for 4 h. 100 μL of solubilization solution (10% SDS in 0.01 M HCl) was added to each well. The microplate was left in the incubator for 24 h. Absorbances at 550 nm were measured on a microplate reader. IC_{50} values (concentration required to reduce the absorbance by 50% compared to the controls) of each complex were determined by the dose dependence of surviving cells after exposure to the platinum(II) complex for 48 h.

Fluorescence and confocal microscopy: A monolayer culture of KB-3-1 cells was incubated in the absence and presence of **1** (18 μM) or cisplatin (22 μM) in 5% CO_2 at 37°C for 72 h. An aliquot of the solution (1 mL) was stained with an AO/EB solution (40 μL, 50 μg mL^{-1} AO, 50 μg mL^{-1} EB in phosphate buffer). Staining was performed prior to examination with a laser confocal microscope (Zeiss Axiovert 100 M).

DNA fragmentation assay: The cancer cells (KB-3-1) were cultured at a concentration of approximately 2×10^5 cells mL^{-1}. Complex **1** (18.4 μM) or **2** (0.39 mM) was added to the culture medium (10% fetal calf serum (FCS, Gibco), 1% Sigma A-7292 Antibiotic and Antimycotic Solution). A DNA sample in the absence of the platinum(II) complex was used as negative control. After treatment, the cultures were incubated in 5% CO_2 at 37°C, and the cells were sampled at 6, 12, and 24 h intervals. The genomic DNA was extracted according to the literature method,[66] and analyzed by electrophoresis with a 1% (w/v) agarose gel.

Flow cytometric analysis: Flow cytometry measurements were performed with an EPICS XL cytometer (Coulter Corporation, Miami, FL) equipped with an argon laser. The sheath fluid was an isotonic solution (Isoflow Coulter 8547008, Coulter Corporation). An excitation wavelength of 488 nm at 15 mW was used. About 10000 cells were analyzed in each sample. Cancer cells (HeLa cell line) were cultured at a concentration of approximately 2×10^5 cells mL^{-1}. Complex **1** (18.4 μM) or **2** (0.39 mM) was added to the cultures. *Staurosporin streptomyces* was used as positive control. After treatment, the cultures were incubated in 5% CO_2 at 37°C. Cells were collected at 12 and 18 h intervals. The genomic DNA was extracted according to the literature method,[66] and analyzed by Annexin V plus PI staining.

Preparation of $[Pt(CNN)(4\text{-dpt})]PF_6$ (1): A suspension of 4-dpt (0.041 g, 0.22 mmol) and [Pt(CNN)Cl] (0.10 g, 0.22 mmol) in an acetonitrile/methanol mixture (1/1, 40 mL) was refluxed for 24 h under a nitrogen atmosphere to give a clear orange solution. Addition of methanolic NH_4PF_6 (0.10 g, 0.65 mmol) gave a yellow precipitate, which was washed with diethyl ether. Recrystallization by diffusion of diethyl ether into an acetonitrile solution afforded a yellow crystalline solid. Yield: 0.14 g, 83%. FABMS: *m*/*z* 614 [M^+], 426 [M^+–(4-dpt)]. ^{1}H NMR (500 MHz, [D$_6$]DMSO: 6.32 (s, 1H), 6.80–7.32 (m, 5H), 7.52 (m, 1H), 7.70–7.82 (m, 3H), 8.05–8.48 (m, 6H), 8.56 (m, 1H), 8.84 (m, 1H), 9.25 (m, 1H). IR (Nujol): $\tilde{\nu}$ = 3370 (w, N–H), 1603 cm^{-1} (s, C=N). Elemental analysis calcd for $C_{24}H_{19}N_8PF_6Pt$: C, 37.95; H, 2.52; N, 14.75; found: C, 38.15; H, 2.60; N, 14.73. UV/Vis (CH_3CN): λ/nm (ε_{max}/dm^3 mol^{-1} cm^{-1}) 420 (1100), 320 (1.36×10^4), 268 (4.22×10^4).

Acknowledgement

This work is supported by the Areas of Excellence Scheme established under the University Grants Committee of the Hong Kong Special Administrative Region, China (AoE/P-10/01), and The University of Hong Kong (Generic Drugs Research Program and University Development fund) HK.

[1] K. E. Erkkila, D. T. Odom, J. K. Barton, *Chem. Rev.* **1999**, *99*, 2777–2795.
[2] C. A. Claussen, E. C. Long, *Chem. Rev.* **1999**, *99*, 2797–2816.
[3] E. R. Jamieson, S. J. Lippard, *Chem. Rev.* **1999**, *99*, 2467–2498.
[4] M. Howe-Grant, S. J. Lippard, *Biochemistry* **1979**, *18*, 5762–5769.
[5] M. J. Clarke, F. Zhu, D. R. Frasca, *Chem. Rev.* **1999**, *99*, 2511–2534.
[6] D. S. Sigman, *Acc. Chem. Res.* **1986**, *19*, 180–186.
[7] C. M. Che, M. Yang, K.-H. Wong, H.-L. Chan, W. Lam, *Chem. Eur. J.* **1999**, *5*, 3350–3356.
[8] C. M. Che, R. W. Y. Sun, W. Y. Yu, C. B. Ko, N. Zhu, H. Z. Sun, *Chem. Commun.* **2003**, 1718–1719.
[9] L. Z. Wu, T. C. Cheung, C. M. Che, K. K. Cheung, M. H. W. Lam, *Chem. Commun.* **1998**, 1127–1128.
[10] H. Q. Liu, T. C. Cheung, S. M. Peng, C. M. Che, *J. Chem. Soc. Chem. Commun.* **1995**, 1787–1788.
[11] G. Lowe, A. S. Droz, T. Vilaivan, G. W. Weaver, J. J. Park, J. M. Pratt, L. Tweedale, L. R. Kelland, *J. Med. Chem.* **1999**, *42*, 3167–3174.
[12] D. R. McMillin, K. M. McNett, *Chem. Rev.* **1998**, *98*, 1201–1219.
[13] D. Goodsell, M. L. Kopka, R. E. Dickerson, *Biochemistry* **1995**, *34*, 4983–4993.
[14] M. L. Kopka, C. Yoon, D. Goodsell, P. Pjura, R. E. Dickerson, *Proc. Natl. Acad. Sci. USA* **1985**, *82*, 1376–1380.
[15] M. Coll, C. A. Frederick, A. H. Wang, J. Rich, *Proc. Natl. Acad. Sci. USA* **1987**, *84*, 8385–8389.
[16] T. A. Larsen, D. S. Goodsell, D. Cascio, K. Grzeskowiak, R. E. Dickerson, *J. Biomol. Struct.* **1989**, *7*, 477–497.

[17] P. E. Pjura, K. Grzeskowiak, R. E. Dickerson, *J. Mol. Biol.* **1987**, *197*, 257–271.
[18] M. K. Teng, N. Usman, C. A. Frederick, A. H. Wang, *Nucleic Acids Res.* **1988**, *16*, 2671–2690.
[19] M. A. Carrondo, M. Coll, J. Aymami, A. H. Wang, G. A. Marel, J. H. Boom, A. Rich, *Biochemistry* **1989**, *28*, 7849–7859.
[20] A. D. Burrows, C.-W. Chan, M. M. Chowdhry, J. E. McGrady, D. M. P. Mingos, *Chem. Soc. Rev.* **1995**, *24*, 329–339.
[21] J. H. K. Yip, Suwarno, J. J. Vittal, *Inorg. Chem.* **2000**, *39*, 3537–3543.
[22] H. Q. Liu, T. C. Cheung, C. M. Che, *Chem. Commun.* **1996**, 1039–1040.
[23] D. R. McMillin, F. Liu, K. A. Meadows, T. K. Aldridge, B. P. Hudson, *Coord. Chem. Rev.* **1993**, *132*, 105–112.
[24] P. B. Dervan, R. W. Burli, *Curr. Opin. Chem. Biol.* **1999**, *3*, 688–693.
[25] C.-W. Chan, D. M. P. Mingos, A. J. P. White, D. J. Williams, *Polyhedron* **1996**, *15*, 1753–1767.
[26] E. C. Constable, R. P. G. Henney, T. A. Leese, D. A. Tocher, *J. Chem. Soc. Chem. Commun.* **1990**, 513–515.
[27] E. Forsellini, G. Bombieri, B. Crociani, T. Boschi, *J. Chem. Soc. D.* **1970**, 1203–1204.
[28] S.-W. Lai, M. C.-W. Chan, T.-C. Cheung, S.-M. Peng, C.-M. Che, *Inorg. Chem.* **1999**, *38*, 4046–4055.
[29] S.-W. Lai, M. C.-W. Chan, K.-K. Cheung, C.-M. Che, *Organometallics* **1999**, *18*, 3327–3336.
[30] C. V. Kumar, E. H. Asuncion, *J. Am. Chem. Soc.* **1993**, *115*, 8547–8553.
[31] W. I. Sundquist, S. J. Lippard, *Coord. Chem. Rev.* **1990**, *100*, 293–322.
[32] H.-L. Chan, D.-L. Ma, M. Yang, C.-M. Che, *ChemBioChem* **2003**, *4*, 62–68.
[33] J. D. McGhee, P. H. Hippel, *J. Mol. Biol.* **1974**, *86*, 469–489.
[34] J. D. McGhee, *Biopolymers* **1976**, *15*, 1345–1375.
[35] V. M. Miskowski, V. H. Houlding, *Coord. Chem. Rev.* **1991**, *111*, 145–152.
[36] G. Cohen, H. Eisenberg, *Biopolymers* **1969**, *8*, 45–55.
[37] B. Åkerman, *J. Am. Chem. Soc.* **1999**, *121*, 7292–7301.
[38] S. Neidle, L. H. Pearl, J. V. Skelly, *Biochem. J.* **1987**, *243*, 1–13.
[39] C. J. Shelton, M. M. Harding, A. S. Prakash, *Biochemistry* **1996**, *35*, 7974–7982.
[40] C. A. Franklin, J. V. Fry, J. G. Collins, *Inorg. Chem.* **1996**, *35*, 7541–7545.
[41] M. Cusumano, M. L. Di Pietro, A. Giannetto, *Inorg. Chem.* **1999**, *38*, 1754–1758.
[42] M. Howe-Grant, K. C. Wu, W. R. Bauer, S. J. Lippard, *Biochemistry* **1976**, *15*, 4339–4346.
[43] H.-Q. Liu, S.-M. Peng, C.-M. Che, *J. Chem. Soc. Chem. Commun.* **1995**, 509–510.
[44] M. L. Kopka, C. Yoon, D. Goodsell, P. Pjura, R. E. Dickerson, *J. Mol. Biol.* **1985**, *183*, 553–563.
[45] D. L. Boger, S. L. Colletti, T. Honda, R. F. Menezes, *J. Am. Chem. Soc.* **1994**, *116*, 5607–5618.
[46] J. K. Barton, A. T. Danishefsky, J. M. Goldberg, *J. Am. Chem. Soc.* **1984**, *106*, 2172–2176.
[47] Y. Jenkins, J. K. Barton, *J. Am. Chem. Soc.* **1992**, *114*, 8736–8738.
[48] F. G. Loontiens, P. Regenfuss, A. Zechel, L. Dumortier, R. M. Clegg, *Biochemistry* **1990**, *29*, 9029–9039.
[49] K. J. Breslauer, D. P. Remeta, W. Y. Chou, R. Ferrante, J. Curry, D. Zaunczkowski, J. G. Snyder, L. A. Marky, *Proc. Natl. Acad. Sci. USA* **1987**, *84*, 8922–8926.
[50] L. A. Marky, K. S. Blumenfeld, K. J. Breslauer, *Nucleic Acids Res.* **1983**, *11*, 2857–2870.
[51] G. Manzini, M. L. Barcellona, M. Avitabile, F. Quadrifoglio, *Nucleic Acids Res.* **1983**, *11*, 8861–8876.
[52] D. S. Pilch, M. A. Kirolos, X. Y. Liu, G. E. Plum, K. J. Breslauer, *Biochemistry* **1995**, *34*, 9962–9976.
[53] D. Suh, J. B. Chaires, *Bioorg. Med. Chem* **1995**, *3*, 723–728.
[54] J. M. Kelly, D. J. McConnell, C. OhUigin, A. B. Tossi, A. K. D. Mesmaeker, A. Masschelein, J. Nasielski, *J. Chem. Soc. Chem. Commun.* **1987**, 1821–1823.
[55] A. K. D. Mesmaeker, G. Orellana, J. K. Barton, N. J. Turro, *Photochem. Photobiol.* **1990**, *52*, 461–472.
[56] A. K. D. Mesmaeker, G. Orellana, J. K. Barton, N. J. Turro, *Photochem. Photobiol.* **1991**, *54*, 499–509.
[57] M. M. Feeney, J. M. Kelly, A. B. Tossi, A. K. D. Mesmaeker, J. P. Lecomte, *J. Photochem. Photobiol.* **1994**, *23*, 69–78.
[58] S. Akiyama, A. Fojo, J. A. Hanover, I. Pastan, M. M. Gottesman, *Somatic Cell Mol. Genet.* **1985**, *11*, 117–126.
[59] D. W. Shen, C. Cardarelli, J. Hwang, M. Cornwell, N. Richert, S. Ishii, I. Pastan, M. M. Gottesman, *J. Biol. Chem.* **1986**, *261*, 7762–7770.
[60] R. A. Schwartzman, J. A. Cidlowski, *Endocr. Rev.* **1993**, *14*, 133–151.
[61] I. Vermes, C. Haanen, *Adv. Clin. Chem.* **1994**, *31*, 177–246.
[62] R. V. Furth, T. L. V. Zwet, *J. Immunol. Methods* **1988**, *108*, 45–51.
[63] J. S. Savill, P. M. Henson, J. E. Henson, C. Haslett, M. J. Walport, A. H. Wyllie, *J. Clin. Invest.* **1989**, *83*, 865–875.
[64] N. A. Thornberry, Y. Lazebnik, *Science* **1998**, *281*, 1312–1316.
[65] J. A. Hickman, *Cancer Metastasis Rev.* **1992**, *11*, 121–139.
[66] J. Sambrook, E. F. Fritsch, T. E. Maniatis, *Molecular Cloning, A Laboratory Manual*, 2nd ed., Cold Spring Harbor Laboratory, **1989**, E.3, E.10.
[67] J. K. Barton, J. M. Goldberg, C. V. Kumar, N. J. Turro, *J. Am. Chem. Soc.* **1986**, *108*, 2081–2088.
[68] F. Kröhnke, *Synthesis* **1976**, 1–24.
[69] T.-C. Cheung, K.-K. Cheung, S.-M. Peng, C.-M. Che, *J. Chem. Soc. Dalton Trans.* **1996**, 1645–1651.
[70] G. M. Sheldrick, SHELXS-97, Program for Crystal Structure Analysis, University of Göttingen, Göttingen (Germany), **1997**.
[71] J. B. Chaires, N. Dattagupta, D. M. Crothers, *Biochemistry* **1982**, *21*, 3933–3940.
[72] J. Sambrook, E. F. Fritsch, T. E. Maniatis, *Molecular Cloning, A Laboratory Manual*, 2nd ed., Cold Spring Harbor Laboratory, **1989**, 5.31.
[73] W. Chen, Y. Lee, H. Wang, G. G. Yu, W. Jian, W. Zhou, Y. Zeng, *J. Cancer Res. Clin. Oncol.* **1992**, *119*, 46–48.
[74] S. J. Busch, R. L. Barnhart, G. A. Martin, M. A. Flanagan, R. L. Jackson, *J. Biol. Chem.* **1990**, *265*, 22474–22479.
[75] X. H. Wang, R. W. Masters, Y. C. Wong, K. F. Lo, S. W. Tsao, *Anticancer Res.* **2001**, *21*, 403–408.

Received: March 18, 2003
Revised: July 23, 2003 [F4964]